



# Pathogen sensing device based on 2D MoS<sub>2</sub>/graphene heterostructure.

Estefanía Enebral-Romero<sup>a,b</sup>, Laura Gutiérrez-Gálvez<sup>a</sup>, Rafael Del Caño<sup>a</sup>,  
Manuel Vázquez Sulleiro<sup>b</sup>, Alicia Naranjo<sup>b</sup>, I. Jénifer Gómez<sup>c</sup>, Félix Pariente<sup>a</sup>,  
Emilio M. Pérez<sup>b</sup>, Tania García-Mendiola<sup>a,d,\*</sup>, Encarnación Lorenzo<sup>a,b,d,\*</sup>

<sup>a</sup> Departamento de Química Analítica, Universidad Autónoma de Madrid, 28049 Madrid, Spain

<sup>b</sup> IMDEA-Nanociencia, Ciudad Universitaria de Cantoblanco, 28049 Madrid, Spain

<sup>c</sup> Department of Condensed Matter Physics, Faculty of Science, Masaryk University, Kotlářská 2, 61137 Brno, Czech Republic

<sup>d</sup> Institute for Advanced Research in Chemical Sciences (IAdChem), Ciudad Universitaria de Cantoblanco, Universidad Autónoma de Madrid, 28049 Madrid, Spain

## ARTICLE INFO

### Keywords:

Covalent heterostructures

f-MoS<sub>2</sub>

Electrografting

SARS-CoV-2

Aptasensor

## ABSTRACT

In this work we propose a new methodology for selective and sensitive pathogen detection based on a 2D layered heterostructured biosensing platform. As a proof of concept, we have chosen SARS-CoV-2 virus because the availability of new methods to detect this virus is still a great deal of interest. The prepared platform is based on the covalent immobilization of molybdenum disulphide functionalized with a diazonium salt (f-MoS<sub>2</sub>) onto graphene screen-printed electrodes (GPH SPE) by electrografting of the diazonium salt. This chemistry-based method generates an improved heterostructured biosensing platform for aptamer immobilization and aptasensor development. Electrochemical impedance spectroscopy (EIS) is used to obtain the signal response of the device, proving the ability of the sensor platform to detect the virus. SARS-CoV-2 spike RBD recombinant protein (SARS-CoV-2 S1 protein) has been detected and quantified with a low detection limit of 2.10 fg/mL. The selectivity of the developed biosensor has been confirmed after detecting the S1 protein even in presence of other interfering proteins. Moreover, the ability of the device to detect SARS-CoV-2 S1 protein has been also tested in nasopharyngeal swab samples.

## 1. Introduction

The physical stack of different 2D materials is the root of the field of van der Waals heterostructures (vdWH) [1]. The most widespread method for the synthesis of heterostructures of bidimensional materials is the direct growth of one material on top of the other by chemical vapor deposition (CVD) or van der Waals epitaxy [2,3]. This method has obvious limitations in that the base material has to be stable under the synthetic conditions of the top material, and that each heterostructure requires optimization of the synthetic parameters. Alternatively, one can manually stack one material on top of the other [4]. Both methods are strictly limited to one device at a time and to interfacing the 2D materials through van der Waals forces.

One of the fields where vdWH have shown promise for application is in sensing. In particular, MoS<sub>2</sub>/graphene or MoS<sub>2</sub>/r-GO heterostructures have received a lot of attention, most often as photodetectors [5]. Chemical sensing can also be enhanced by the formation of MoS<sub>2</sub>/graphene vdWH. To name just a couple of prominent examples, Cho

et al. described a flexible sensor based on MoS<sub>2</sub> interfaced with patterned graphene electrodes for the sensing of NO<sub>2</sub> at ppm level [6]. Meanwhile, Pham et al. built a stack of monolayer MoS<sub>2</sub> over graphene using physical methods, which resulted in significant n-doping of the graphene layer. According to the authors, it is this charge-transfer phenomenon in the heterostructure that results in significantly improved performance in chemical sensing of toluene, where the MoS<sub>2</sub>/graphene based sensor shows both higher sensitivity and better signal-to-noise ratio compared to either of the single component sensors (MoS<sub>2</sub> or graphene) in the same Field Effect Transistor (FET) configuration [7].

Some of us recently reported a method to build covalently-linked MoS<sub>2</sub>/graphene heterostructures using a molecular “Velcro” that attaches on one end to MoS<sub>2</sub>, using maleimide-thiol chemistry [8,9], and on the other end to graphene, using diazonium chemistry [10]. This chemistry-based method to build heterostructures allows for precise control of the distance and chemical nature of the interface between materials, which directly determines their electronic communication

\* Corresponding authors at: Departamento de Química Analítica, Universidad Autónoma de Madrid, 28049 Madrid, Spain.

E-mail addresses: [tania.garcia@uam.es](mailto:tania.garcia@uam.es) (T. García-Mendiola), [encarnacion.lorenzo@uam.es](mailto:encarnacion.lorenzo@uam.es) (E. Lorenzo).

<https://doi.org/10.1016/j.snb.2023.134105>

Received 31 March 2023; Received in revised form 6 June 2023; Accepted 6 June 2023

Available online 10 June 2023

0925-4005/© 2023 The Author(s). Published by Elsevier B.V. This is an open access article under the CC BY-NC-ND license (<http://creativecommons.org/licenses/by-nc-nd/4.0/>).

and is, therefore, crucial for function [11]. Moreover, the method is remarkably simple and robust, with all processes based on simple manipulation of suspensions, and the reactions taking place at or near room temperature and under ambient atmosphere. These features in principle make it a particularly suitable method to benefit from the synergy of MoS<sub>2</sub>/graphene chemical sensors without the need for complex nanofabrication technologies. With this in mind, we set out to explore the sensing abilities of commercially available graphene electrodes after covalent functionalization with MoS<sub>2</sub>.

Nowadays, there is great interest in the scientific world in developing new alternative methodologies to traditional ones to detect pathogens rapidly and efficiently. One of the most studied viruses in recent years is SARS-CoV-2, that causes the global pandemic experienced since 2019, declared by the World Health Organization (WHO) as COVID-19, a respiratory disease with a very high capacity to spread [12]. SARS-CoV-2 is a betacoronavirus with high similarity with the SARS-CoV, MERS-CoV, and two other coronavirus. This virus has a spherical structure of single-stranded RNA that encodes five structural proteins, including the S or spike protein, which allows the union between the virus membrane and the host respiratory epithelium cells [13]. The most widely used methodologies for early detection of the virus, known worldwide as PCR (Polymerase Chain Reaction) and antigen tests, are based on the detection of the viral genome or the S protein, respectively. Despite the high sensitivity of PCR and the low cost and short analysis time of antigen tests, the former suffers from long analysis times, high cost, and the need of qualified personnel, while the latter typically shows relatively low sensitivity [14].

Recently, numerous studies have focused on the use of biosensors as an alternative to traditional methodologies due to their simplicity, low cost, selectivity, and sensitivity. One of the main advantages of these devices is the possibility of studying all types of analytes, from DNA or RNA sequences to antibodies or even proteins. In this context, several works based on the development of DNA biosensors for the detection of the SARS-CoV-2 ORF1ab or RdRp sequences, and aptasensors for spike protein detection have been reported [15–19]. The latest is one of the most attractive strategies and an area to be exploited. In the aptamer biosensors or aptasensors, the biological recognition element is an aptamer, a short single-strand oligonucleotide with high stability, that acts as a biorecognition element when it is bonded to the specific target molecule (proteins such as SARS-CoV-2 spike protein) with high selectivity. In these devices, the detection of a specific molecule is based on the biorecognition reaction between the target molecule and the specific aptamer. Among the different methods to obtain the signal response, electrochemistry has proven to be very useful for the detection of viruses, as well as having numerous advantages such as simplicity, fast response, low cost, high sensitivity, and miniaturization capacity. In particular, electrochemical impedance spectroscopy (EIS) is one of the used electrochemical techniques due to its simplicity, its capacity for interfacial analysis in biorecognition reactions, label-free detection, and the fact that it is a steady-state technique. The impedance of a modified electrode is obtained when a potential disturbance is applied in a specific frequency range, by measuring the current intensity [20].

Although some electrochemical biosensors for pathogen detection are reported as a competitive alternative to classical methodologies, some aspect of these devices can be improved, such as sensitivity or stability. In this sense, recently nanomaterials and heterostructures are included in the fabrication of biosensors, and numerous investigations are focused on this area. In contrast, the use of nanostructures can produce non-specific adsorptions and weak binding events between the transducer and the nanomaterial, resulting in low stability and reproducibility. To overcome these drawbacks, different immobilization of the nanostructures by strong interactions as covalent bonding are developed. In this context, we propose the use of molybdenum disulfide functionalized with a diazonium salt (f-MoS<sub>2</sub>) to nanostructure the electrode by covalent binding as an electrochemical platform to further immobilize the recognition agent. The presence of the diazonium

functional group allows the covalent bonding of f-MoS<sub>2</sub> on the electrode surface by the electrografting of f-MoS<sub>2</sub> on GPH SPE, which is achieved by applying a potential that involves the reduction of the diazonium salt and the formation of a free radical capable of reacting with the graphene on the electrode surface [21], but also generates a new heterostructure that serves as an efficient platform for the aptamer immobilization, an essential step on the biosensor development. The signal response of the final device is based on the detection of the recognition reaction between the S1 protein of the SARS-CoV-2 virus, and the aptamer conducted by Electrochemical Impedance Spectroscopy (EIS).

## 2. Material and methods

### 2.1. Reagents, solutions, and apparatus

#### 2.1.1. Reagents

Monobasic sodium phosphate, dibasic sodium phosphate, sodium chloride, acetonitrile, potassium ferrocyanide, potassium ferricyanide, bovine serum albumin, RBD SARS-CoV-2 aptamer thiolated sequence, and other interferents proteins (HER 2, IgG, CEA and p53) shown in Table 1, were supplied by Merck (<https://www.merckgroup.com/>). Interferent 1 (HER2) was purchased as an ELISA kit (Human ErbB2/HER2 DuoSet ELISA DY1129B) by R&D Systems Europe, Ltd. SARS-CoV-2 RBD recombinant spike protein (SARS-CoV-2 S1 protein) was purchased from Sino Biological Europe GmbH (Eschborn, Germany). Bulk MoS<sub>2</sub> was purchased by Sigma Aldrich. N-(4-aminophenyl) maleimide as a precursor for the formation of the diazonium salt was bought from Apollo Scientific.

#### 2.1.2. Solutions

**2.1.2.1. f-MoS<sub>2</sub> solution for the electrografting process.** 1 mg/mL f-MoS<sub>2</sub> dispersion for electrografting process was prepared by suspending 3 mg of f-MoS<sub>2</sub> in 3 mL of acetonitrile (CH<sub>3</sub>CN) and sonicated for 15 min.

**2.1.2.2. Bovine Serum Albumin (BSA) 0.1 % solution.** The 0.1 % BSA solution was prepared by dissolving 10 mg of BSA in 10 mL of phosphate buffer 10 mM and NaCl 0.4 M of pH 7.0 (PBS). Then, it was filtered with a 0.45 µm filter.

**2.1.2.3. Thiolated RBD SARS-CoV-2 aptamer solution.** A 10 µM solution of thiolated RBD SARS-CoV-2 aptamer was prepared using 10 mM buffer phosphate pH 7.0 as solvent after a pre-treatment with dithiothreitol (DTT) and purification by elution through a NAP-10 column of Sephadex G-25 (following manufacturer instructions).

**2.1.2.4. SARS-CoV-2 S1 protein solution.** The stock S1 protein solution of 1 ng/mL was prepared from the stock SARS-CoV-2 S1 protein solution of 0.25 mg/mL (stored at a temperature of −80 °C) and using 10 mM PBS as solvent. Then, the solutions of different concentrations were prepared from the 1 ng/mL stock and stored at a temperature of −20 °C.

#### 2.1.3. Apparatus

Electrochemical measurements (CV and EIS) were performed with an Autolab/PGSTAT 10 potentiostat from EcoChemie with GPES 4.9 and the FRA software. As interface a screen-printed connector was used and as transducers graphene screen-printed electrodes (DRP-110GPH) were used, both supplied by Methrom DropSens. All the electrochemical studies were performed on a homemade electrochemical cell.

The thermogravimetric analysis (TGA) performed to ensure the correct functionalization of the f-MoS<sub>2</sub> was carried out by a TGA Q500 equipment, supplied by TGA instruments.

For the characterization of the developed sensing platform by atomic force microscopy (AFM) a Dimension Icon system in tapping mode was used (Bruker, Germany), using a RTESPA-150 probe (150 kHz; 6 N/m,

**Table 1**

Biological reagents used in this work.

Biological reagents used		
Thiolated RBD SARS-CoV-2 aptamer	5'-SH-C <sub>6</sub> H <sub>12</sub> -CAGCACCGACCTTGTGCTTTGGGAGTGCTGGTCCAAGGGCGTTAATGGACA	apt-SH
SARS-CoV-2 spike RBD recombinant protein	Analyte	S1
HER2 protein	Interferent 1	HER2
P53 protein	Interferent 2	P53
IgG protein	Interferent 3	IgG
CEA protein	Interferent 4	CEA

(Bruker, Germany). The images were analyzed in Gwyddion 2 [22].

In the case of scanning electron microscopy (SEM) and energy dispersive X-Ray Spectroscopy (EDX), a FESEM Auriga, Carl Zeiss scanning electron microscope coupled to an EDX spectrometer was used. The characterization was performed at low voltage (2.5 kV) and current (10 pA).

X-ray photoelectron spectroscopy (XPS) was carried out in an equipment containing an Axis Supra spectrometer (Kratos Analytical LTD., UK) working under ultra-high vacuum conditions ( $5 \times 10^{-10}$  mbar base pressure). Survey XPS spectra was taken at a pass energy of 80 eV.

Finally, Raman measurements were carried out using a Bruker Senterra confocal Raman microscope (Bruker Optic, Ettlingen, Germany, resolution  $3\text{--}5\text{ cm}^{-1}$ ) under the following parameters: NA objective 0.75, 50X; 532 nm laser excitation and 2 mW. The images obtained were performed on an Olympus microscope with a 50X objective lens.

## 2.2. Procedures

### 2.2.1. Molybdenum disulphide functionalized with diazonium salt (f-MoS<sub>2</sub>) synthesis

f-MoS<sub>2</sub> was produced by liquid phase exfoliation of bulk MoS<sub>2</sub> in N-Methyl-2-pyrrolidone (NMP), using an ultrasonic probe (Vibracell 75115, Bioblock Scientific, 500 W) for one hour, at 35 % of amplitude. Black NMP suspension was centrifuged for 30 min at 5000 rpm (2744 g) in an Allegra X-15R Beckman Coulter centrifuge (FX6100 rotor, 20°C), and the olive-colored supernatant was filtered with Omnipore 0.45 µm PTFE membrane filters. The sample was washed by redispersing the material on 20 mL of acetonitrile (CH<sub>3</sub>CN), with a brief sonication and filtering the material again. This redispersion process is repeated for acetonitrile and isopropanol (i-PrOH) three times per solvent, and the exfoliated pristine material (p-MoS<sub>2</sub>) was obtained. The general procedure to obtain the functionalized material was carried out by dispersing 1 mmol of N-(4-diazophenyl) maleimide into a 0.4 mg/mL p-MoS<sub>2</sub> dispersion (8 mg of pristine material in 20 mL of dry CH<sub>3</sub>CN). Mixture was stirred for 16 h at room temperature protected from light. Finally, the black suspension was filtered and washed with CH<sub>3</sub>CN, as previously described, obtaining the functionalized material, f-MoS<sub>2</sub>.

N-(4-diazophenyl) maleimide was synthesized as it was previously described [10]. Very briefly, 0.25 mM N-(4-aminophenyl) maleimide solution was slowly cannulated into 0.38 mM nitronium tetrafluoroborate solution, on a Schlenk flask under argon atmosphere, using 20 mL of dry CH<sub>3</sub>CN as solvent for each solution. Mixture was stirred for 1 h at  $-40^\circ\text{C}$  and after that, it was warmed up to  $0^\circ\text{C}$  for 2 h. Finally, the resulting solution was poured into 500 mL of cool diethyl ether, and the precipitate was filtered, washed three times with 50 mL of diethyl ether, and dried under vacuum.

## 2.3. Aptasensor development

### 2.3.1. Electrografting process of f-MoS<sub>2</sub> on graphene screen-printed electrodes (GPH SPE)

Graphene screen-printed electrodes (GPH SPE) were nanostructured by electrografting process of molybdenum disulphide functionalized with diazonium salt (f-MoS<sub>2</sub>). For this purpose, 15 consecutive scans from  $-1.5\text{ V}$  to  $1.0\text{ V}$  at  $100\text{ mV/s}$  in  $1\text{ mg/mL}$  f-MoS<sub>2</sub> solution in CH<sub>3</sub>CN

were applied on GPH SPE electrodes. The process was carried out in an ice bath and purged with nitrogen. The resulting platform is denoted in the text as GPH SPE/f-MoS<sub>2</sub>.

## 2.4. Aptamer immobilization

GPH SPE/f-MoS<sub>2</sub> platform was modified by drop casting  $10\text{ }\mu\text{L}$  of  $10.0\text{ }\mu\text{M}$  thiolated RBD SARS-CoV-2 aptamer (apt-SH) and kept for 24 h at room temperature (GPH SPE/f-MoS<sub>2</sub>/apt-SH). Then, the non-specific binding sites of the surface were blocked by adding  $10\text{ }\mu\text{L}$  of 0.1 % Bovine Serum Albumin (BSA) for 30 min and then the aptasensor developed was washed with Milli-Q water. The sensing platform developed is named as GPH SPE/f-MoS<sub>2</sub>/apt-SH/BSA.

## 2.5. Biorecognition reaction and electrochemical detection of SARS-CoV-2 S1 protein

The GPH SPE/f-MoS<sub>2</sub>/apt-SH/BSA platform was incubated with  $10\text{ }\mu\text{L}$  of different concentrations of SARS-CoV-2 S1 protein (in  $10\text{ mM}$  phosphate buffer, PBS) solution for 1 h at  $37^\circ\text{C}$  in a humidity chamber. The signal response was obtained by Cyclic Voltammetry (CV) and Electrochemical Impedance Spectroscopy (EIS) immersing the modified electrode in a solution of  $10\text{ mM}$  K<sub>3</sub>Fe(CN)<sub>6</sub> with  $10\text{ mM}$  K<sub>4</sub>Fe(CN)<sub>6</sub> in PB  $0.1\text{ M}$  pH 7.0, and cycling the potential from  $-1.0$  to  $1.2\text{ V}$  (2 scans) at  $100\text{ mV/s}$  for CV, or applying a potential of  $0.12\text{ V}$  in a frequency range from  $100\text{ kHz}$  to  $0.01\text{ Hz}$  with a sinusoidal voltage of  $10\text{ mV}$  amplitude for EIS. To interpretate the results obtained with the EIS measures, impedance values ( $Z$ ) are represented in a Nyquist plot ( $-Z''$  vs.  $Z'$ ) and adjusted to an equivalent electric circuit (see inset of Fig. 4). This equivalent circuit consists of the resistance of the connector ( $R_s$ ), the resistance between the electrolyte and the substances immobilized on the surface of the electrode ( $R_{ct}$ ), a Warburg impedance element that represents the diffusion of the redox solution to the electrode ( $Z_W$ ) and a constant phase element (the electrode modified) that simulates the non-ideal capacitor behaviour (CPE).

## 2.6. Detection of SARS-CoV-2 S1 protein in human serum samples

SARS-CoV-2 S1 protein was determined in human serum samples spiked with SARS-CoV-2 S1 protein to study the matrix effect as well as to confirm the applicability of the aptasensor. Human serum spiked samples were prepared at a final concentration of  $100\text{ fg/mL}$  SARS-CoV-2 S1 protein using human serum as solvent (supplied by Merck). Secondly,  $10.0\text{ }\mu\text{L}$  of this solution were incubated with the heterostructured platform (GPH SPE/f-MoS<sub>2</sub>/apt-SH/BSA) on the electrode surface. Then, the recognition reaction described above was carried out. Next, the electrodes were washed with water to remove non-adsorbed material and the EIS signal was recorded as it is described above. Finally, the SARS-CoV-2 S1 protein concentration was calculated from the  $R_{ct}$  signal average value of three determinations obtained using the calibration plot ( $R_{ct} = 0.756 \cdot [\text{S1 protein}] + 94.0$ ;  $R = 0.987$ ). The recovery was calculated considering the concentration founded and the real concentration of the spiked human serum.



### 2.6.1. Detection of SARS-CoV-2 S1 protein in nasopharyngeal swab samples

SARS-CoV-2 virus was determined in nasopharyngeal swab samples spiked with two different concentrations of SARS-CoV-2 S1 protein (40.0 and 60.0 fg/mL) using 100 fg/mL protein stock solution and PBS 10 mM pH 7.0 as solvent. Then, 10  $\mu$ L of each sample solution were incubated on the surface of the GPH SPE/f-MoS<sub>2</sub>/apt-SH/BSA platform for 1 h at 37 °C. After washing the electrodes, the EIS response was recorded as described above. With the recalculated Rct values and the concentrations obtained after interpolating the impedance on the calibration plot ( $R_{ct} = 0.756 \cdot [S1 \text{ protein}] + 94.0$ ;  $R=0.987$ ) the recovery for each concentration was calculated.

## 3. Results and discussion

In this work we developed a new heterostructured biosensing platform based on the combination of molybdenum disulphide (2D nano-material) with graphene screen-printed electrodes (GPH SPE), used as transducers (high electric conductivity and excellent mechanical properties), to improve the stability, sensitivity, and selectivity of the final sensing platform [23,24]. The development of heterostructures based on the use of f-MoS<sub>2</sub> and diazonium chemistry allow us to control the reactivity, conductivity, and stability of modified electrodes, requiring simple and affordable methodologies and instrumentation, being a good alternative for biosensor development.

The biosensing device has a broad applicability including detection of pathogens. In particular, as case of study due to the current interest in the new methodologies for rapid and easy detection of virus we have applied our biosensing device to the detection of the S1 protein of the SARS-CoV-2 virus.

### 3.1. Synthesis and characterization of f-MoS<sub>2</sub>

The synthesis of the diazonium salt and functionalization of the exfoliated pristine molybdenum disulphide (p-MoS<sub>2</sub>) to get the final molybdenum disulphide functionalized with diazonium salt (f-MoS<sub>2</sub>) material is shown in the experimental section. A more comprehensive characterization can be found in bibliography [10]. Routinely, a thermogravimetric analysis (TGA) was performed for each new batch of p-MoS<sub>2</sub> and f-MoS<sub>2</sub>, to ensure the correct functionalization, (see

**Figure 1S1**). The experiments were running out under airflow, using a temperature ramp of 10 °C/min from 100 to 800 °C.

### 3.2. Aptasensor development and characterization

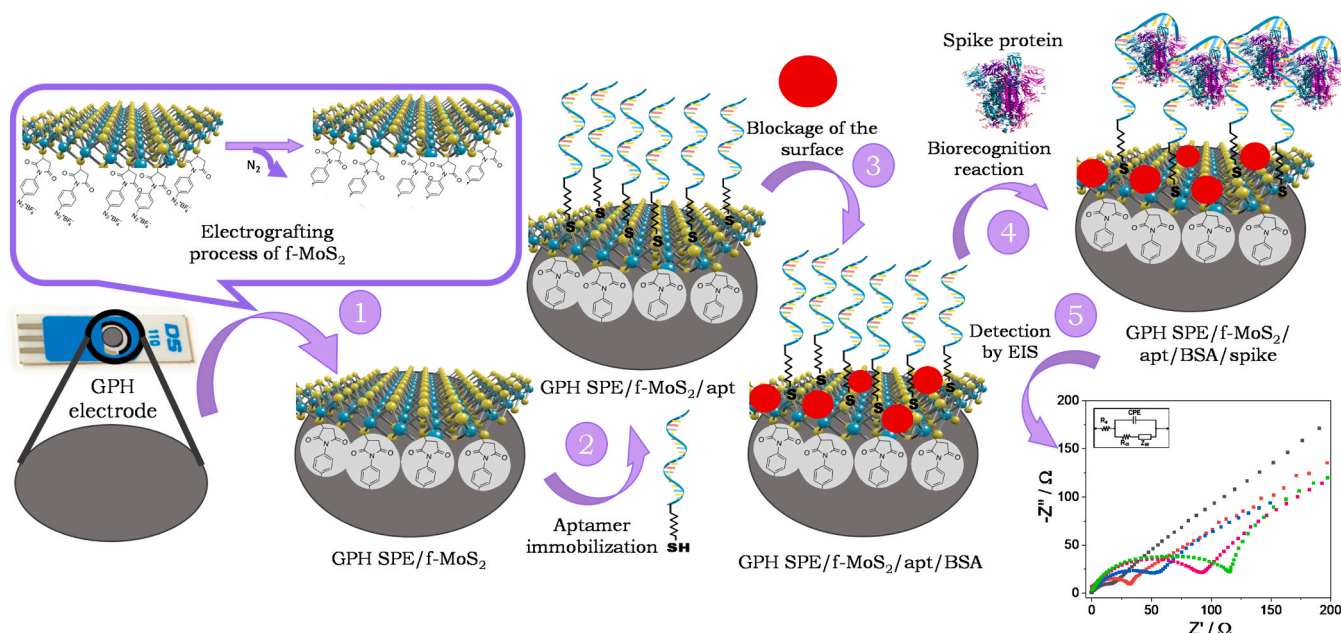
The 2D Graphene/MoS<sub>2</sub> heterostructured biosensing platform is developed by nanostructuration of graphene screen-printed electrodes (GPH SPEs) with molybdenum disulphide functionalized with diazonium salt (f-MoS<sub>2</sub>), and its further modification with an aptamer (see **Scheme 1**) which specifically recognize the S1 protein of the SARS-CoV-2 virus. The recognition reaction is conducted by Electrochemical Impedance Spectroscopy (EIS) allowing SARS-CoV-2 virus detection and quantification.

As can be observed in **Scheme 1**, the first step is electrografting of the diazonium salt of f-MoS<sub>2</sub> on the graphene electrode. This process allows the covalent anchoring of f-MoS<sub>2</sub> to the graphene surface. The electrografting was carried out applying a potential to the f-MoS<sub>2</sub> solution which reduces and forms the aryl radical, favouring the covalent bonding between the graphene electrode surface and the f-MoS<sub>2</sub> (See step 1 of **Scheme 1**).

It is well known that during the electrografting process of diazonium salts in carbon surfaces, the current intensity decreases with the number of scans since the electron transfer is hindered, due to the non-electroactive layer formed with the covalent anchoring[25] This behaviour is observed when the f-MoS<sub>2</sub> is electrografted on GPH SPE as shown in **Fig. 1**, confirming the immobilization of the f-MoS<sub>2</sub> on the electrode surface.

After electrode nanostructuration with f-MoS<sub>2</sub> by electrografting, the immobilization of the thiolated RBD SAR-CoV-2 aptamer, a short single-strand oligonucleotide modified in the 5'-end with a thiol group (apt-SH), was performed due to the ability of this thiolated molecule to eliminate the sulphur vacancies of the f-MoS<sub>2</sub> layer [26]. Then, the heterostructured biosensing platform was characterized by atomic force microscopy (AFM), scanning electron microscopy (SEM), energy dispersive X-Ray spectroscopy (EDX), X-Ray photoelectron spectroscopy (XPS), and Raman spectroscopy.

The AFM and SEM images (see **Fig. 2**) show the changes caused in the morphology of the electrode after the nanostructuration with f-MoS<sub>2</sub> and the immobilization of the aptamer. Bare GPH SPE (**Fig. 2A and 2D**) shows some layers from the graphene of the surface. After the



**Scheme 1.** Scheme followed for the biosensor development for the SARS-CoV-2 S1 protein detection.

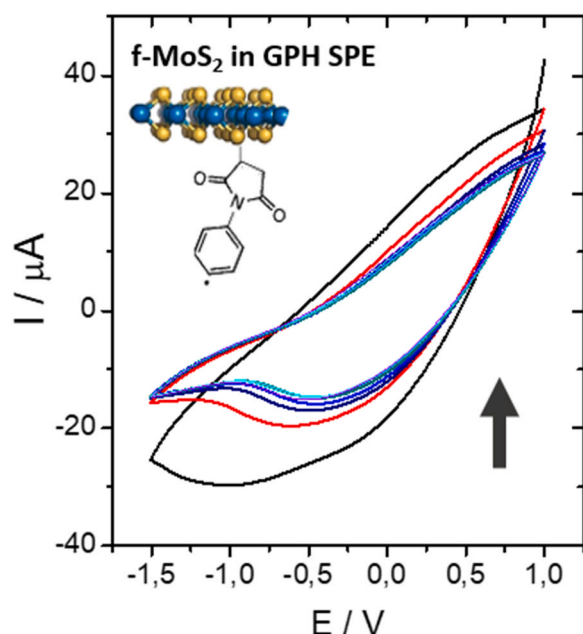


**Fig. 1.** Cyclic Voltammograms of the electrografting process of f-MoS<sub>2</sub> (10 cycles, 100 mV/s, from −1.5 to 1.0 V) on GPH SPE electrodes immersed in 1 mg/mL f-MoS<sub>2</sub> in CH<sub>3</sub>CN solution.

electrografting of f-MoS<sub>2</sub>, GPH SPE/f-MoS<sub>2</sub> (Fig. 2B and 2E), layers of f-MoS<sub>2</sub> appear on the graphene. Finally, the immobilization of the aptamer, GPH SPE/f-MoS<sub>2</sub>/apt-SH (Fig. 2C and 2F), increases the surface roughness of the electrode.

The heterostructured biosensing platform development was also confirmed by EDX (Fig. 2G–I). The presence of carbon from the graphene is observed in all the steps of the fabrication process. After the nanostructuration with f-MoS<sub>2</sub>, the presence of Mo and S is clear. The aptamer immobilization is confirmed by the presence of N, and P from the nitrogenous bases of the aptamer sequence.

In accordance with the EDX data, the XPS spectrum of the bare GPH SPE (Fig. 3A, black line) shows the C 1 s signal from the graphene of the surface. The electrografting of the f-MoS<sub>2</sub> is confirmed by the appearance of the S 2p signal (red line) of the f-MoS<sub>2</sub>. Finally, the aptamer immobilization is demonstrated with the O 1 s, N 1 s, and P 2 s/2p signals observed (blue line) due to the nitrogenous bases of the aptamer [27,28].

The Raman spectrum for the bare electrode (black line of Fig. 3B) shows the characteristics D, G, and 2D bands of the carbon present on the graphene surface at 1350, 1581, and 2718 cm<sup>−1</sup>, respectively. Once the f-MoS<sub>2</sub> is electrografted (red line), the two active Raman modes E<sub>2g</sub> and A<sub>1g</sub> of the molybdenum disulphide are observed at 380 cm<sup>−1</sup> and 406 cm<sup>−1</sup>. After the aptamer immobilization (blue line), some peaks at 1000 cm<sup>−1</sup> appear probably due to the nitrogenous bases of the aptamer sequence [27].

All the results obtained by the different techniques point out a successful electrografting of the f-MoS<sub>2</sub> on the GPH SPE electrode for the electrochemical heterostructured biosensing platform development and further RBD SARS-CoV-2 aptamer immobilization.

### 3.3. SARS-CoV-2 S1 protein detection

The ability of the biosensing platform developed to detect the SARS-CoV-2 S1 protein was studied by Cyclic Voltammetry (CV) and Electrochemical Impedance Spectroscopy (EIS). First of all, after the aptamer immobilization, the surface of GPH SPE/f-MoS<sub>2</sub>/apt-SH platform was blocked with 0.1 % Bovine Serum Albumin (BSA) to avoid unspecific absorptions. Then, different concentrations of the SARS-CoV-2 S1

protein were incubated with the GPH SPE/f-MoS<sub>2</sub>/apt-SH/BSA platform under the optimal condition of time, temperature, and pH (1 h at 37 °C using 10 mM of phosphate buffer (PBS) pH 7.0 solution, see experimental section). Finally, the biorecognition reaction between the aptamer and the SARS-CoV-2 S1 protein was detected electrochemically by immersing it in a solution containing 10 mM K<sub>3</sub>Fe(CN)<sub>6</sub> and 10 mM K<sub>4</sub>Fe(CN)<sub>6</sub> in PB 0.1 M pH 7.0, and recording the Cyclic Voltammograms and the Nyquist plot (see Fig. 4).

The Cyclic Voltammogram (see Fig. 4A) of the bare GPH SPE (black line) shows the characteristics oxidation and reduction peaks of the [Fe(CN)<sub>6</sub>]<sup>3-/4-</sup> redox couple at 0.35 V and −0.072 V respectively, an ΔE<sub>p</sub> of 422 mV and a peak current (I<sub>p</sub>) of 330 μA. When the electrode is nanostructured with f-MoS<sub>2</sub> (red line) the ΔE<sub>p</sub> increases to 439 mV and the I<sub>p</sub> decreases to 249 μA, which means a worsening of the electron transfer due to the formation of a non-electroactive layer on the electrode surface after the covalent bonding between the diazonium salt and the graphene of the electrode. After the immobilization of the RBD SARS-CoV-2 aptamer (blue line), the ΔE<sub>p</sub> and the I<sub>p</sub> values obtained were 533 mV and 234 μA respectively, which again point to a hindering in the electron transfer, that comes from the electrostatic repulsion between the negative charge of the [Fe(CN)<sub>6</sub>]<sup>3-/4-</sup> redox couple and negatively charged aptamer, thus confirming the correct aptamer immobilization. Surface blocking with BSA (pink line) results in a decrease of I<sub>p</sub> to 216 μA, which confirms the correct blockage of the non-specific binding sites of the electrode surface. Finally, after the incubation of the aptasensor with 30 fg/mL of SARS-CoV-2 S1 protein (green line), an increase of ΔE<sub>p</sub> to 629 mV and a decrease of I<sub>p</sub> to 197 μA are observed, due to the steric/conformational restriction of protein molecules that hinders the electron transfer. These results can be confirmed by EIS technique with the Nyquist plots registered, where the diameter of the curve corresponds with the electron-transfer resistance (R<sub>ct</sub>) as it is shown in Fig. 4B. For the bare GPH SPE (black line) a R<sub>ct</sub> value of 17,16 Ω is obtained. With the electrografting of f-MoS<sub>2</sub> (red line), the R<sub>ct</sub> increases to 31,74 Ω, due to the less-electroactive layer formed that hinders the electron transfer. After the aptamer immobilization (blue line), the resistance increases again reaching a value of R<sub>ct</sub> of 51,06 Ω, which indicates the electrostatic repulsion with the redox couple that hinders the electron transfer, and the correct aptamer immobilization. When the surface is blocked with BSA R<sub>ct</sub> increases up to 91,17 Ω, confirming the effective blockage. Finally, when 30 fg/mL of S1 protein is incubated with the biosensor, the R<sub>ct</sub> increases to 121.62 Ω. This result corresponds to the impedance in charge transfer generated by the steric/conformational restriction of the protein causing a barrier that hinders electronic transfer [29,30]. The above results demonstrate the ability of the biosensor to detect the SARS-CoV-2 S1 protein.

In order to demonstrate the robustness of the proposed device for diagnostic purposes, we evaluate the effect of experimental parameters such as the ionic strength and the pH of the incubation buffer for a concentration of 30 fg/mL of SARS-CoV-2 S1 protein. Figure 6 of SI includes the resistances obtained varying the pH (from 6 to 8) (Figure 2ASI) and ionic strength (Figure 2BSI). As can be observed, the signal is quite similar in all the studies carried out confirming the robustness of the platform.

After verifying the ability of the developed biosensor to detect SARS-CoV-2 S1 protein and its robustness, we studied its response to different concentrations of SARS-CoV-2 S1 protein from 5.00 fg/mL to 200 fg/mL. We observe that on increasing protein concentrations, the resistance increases (see Fig. 5A). This phenomenon is also reported by other authors [29] and indicates the inhibition effects of spike protein on the electron transfer between redox probe and the electrode surface. This increase can be attributed to the steric/conformational restriction at the electrode surface with the barrier effect of protein molecules, an inhibition of electron transfer occurred, and thus an increase in resistance is observed [30].

The analytical parameters were determined under the optimal experimental conditions described above. As it is shown in the



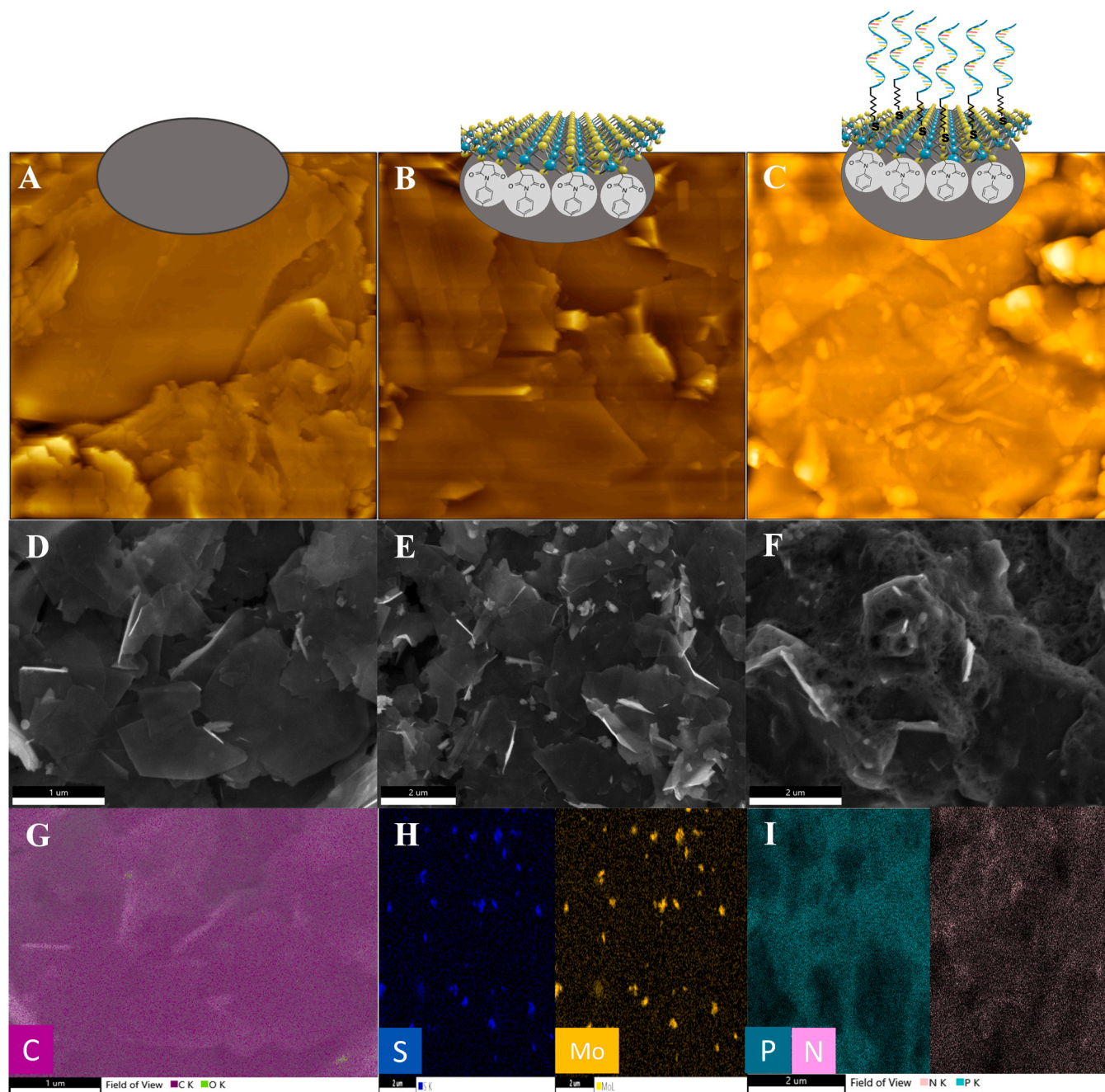


**Fig. 2.**  $5 \times 5 \mu\text{m}$  AFM images (A, B, C), SEM (D, E, F) and EDX (G, H, I) of a bare GPH SPE electrode (A, D, G), GPH SPE/f-MoS<sub>2</sub> (B, E, H) and GPH SPE/f-MoS<sub>2</sub>/apt-SH (C, F, I).

calibration plot of Fig. 5A, there is an increasing linear correlation between the impedance response and the SARS-CoV-2 S1 protein concentration that fits to the linear equation,  $R_{ct} = 0.756 \cdot [\text{S1 protein}] + 94.0$  ( $R=0.987$ ). Values were obtained from the mean of three different measurements for each concentration, with a sensitivity of  $0.756 \Omega/\text{fg}\cdot\text{mL}^{-1}$ . The limit of detection (LOD) and quantification (LOQ) obtained (based on three and ten times the standard deviation of the probe impedance divided by the slope of the calibration line) were  $2.10 \text{ fg/mL}$  and  $7.01 \text{ fg/mL}$ , respectively.

To determine the selectivity of the aptasensor, we studied its response to  $100 \text{ fg/mL}$  of SARS-CoV-2 S1 protein in presence of different potentially interfering proteins, such as HER2, p53, IgG, and CEA at the same concentration (Fig. 5B). The response is not affected by the presence of any protein, confirming its selectivity for SARS-CoV-2 S1

protein. Moreover, the stability of the aptasensor was assessed, with results pointing out that the aptasensor response is stable for two months.

To demonstrate the main role of the electrografted f-MoS<sub>2</sub> in the sensing device performance, we have developed the same aptasensor but using unfunctionalized MoS<sub>2</sub> flakes (p-MoS<sub>2</sub>) directly drop-casted on the graphene electrode surface. That is a control experiment where the MoS<sub>2</sub>/Graphene heterostructure is built by physisorption, without the covalent linkage. The  $R_{ct}$  value obtained at each step of the biosensor development (Figure 3SIA) indicates that this new platform shows similar results to those obtained when the MoS<sub>2</sub> flakes are electrografted. However, less sensitivity ( $R_{ct} = 0.0422 \cdot [\text{S1 protein}] + 43.4$ ) and higher detection and quantification limits are achieved,  $1.96 \text{ pg/mL}$  and  $6.53 \text{ pg/mL}$ , respectively. Moreover, when we evaluate a concentration

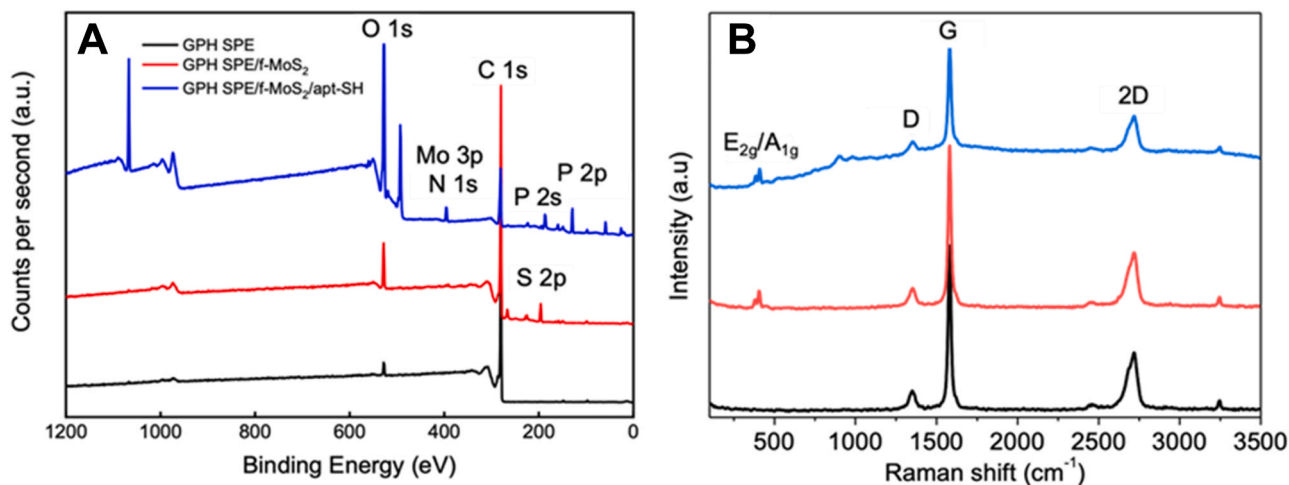


Fig. 3. XPS (A) and Raman (B) spectrum of a bare GPH SPE (black line), GPH SPE/f-MoS<sub>2</sub> (red line), and GPH SPE/f-MoS<sub>2</sub>/apt-SH (blue line).

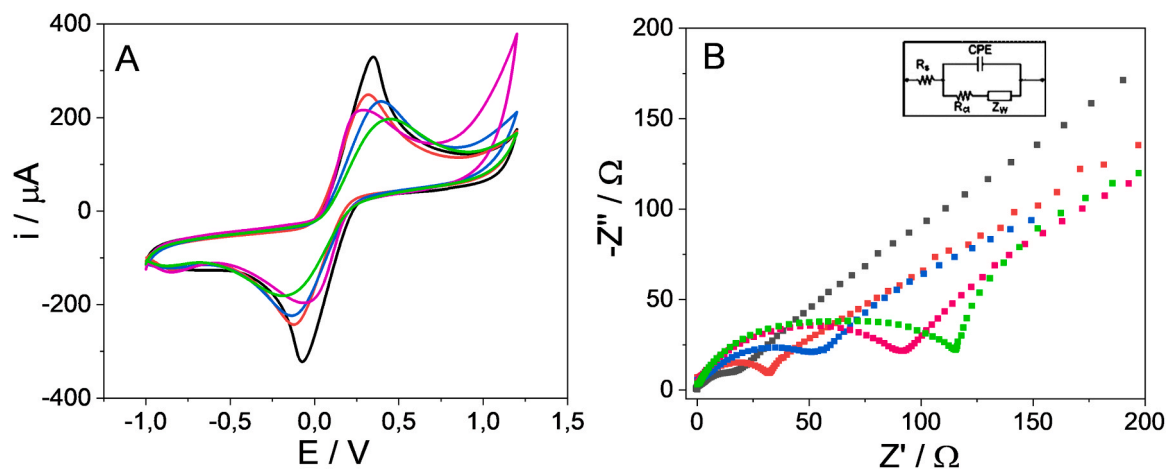


Fig. 4. Cyclic Voltammograms (A) and Nyquist plot (B) of each step on the aptasensor development: bare GPH SPE (black line), GPH SPE/f-MoS<sub>2</sub> (red line), GPH SPE/f-MoS<sub>2</sub>/apt-SH (blue line), GPH SPE/f-MoS<sub>2</sub>/apt-SH/BSA (pink line) and GPH SPE/f-MoS<sub>2</sub>/apt-SH/BSA/S1 30 fg/mL (green line) in 10 mM K<sub>3</sub>Fe(CN)<sub>6</sub> with 10 mM K<sub>4</sub>Fe(CN)<sub>6</sub> in PB 0.1 M pH 7.0. Scan rate CV: 100 mV/s. EIS conditions: 0.12 V, 100 kHz to 0.01 Hz, and 10 mV amplitude.

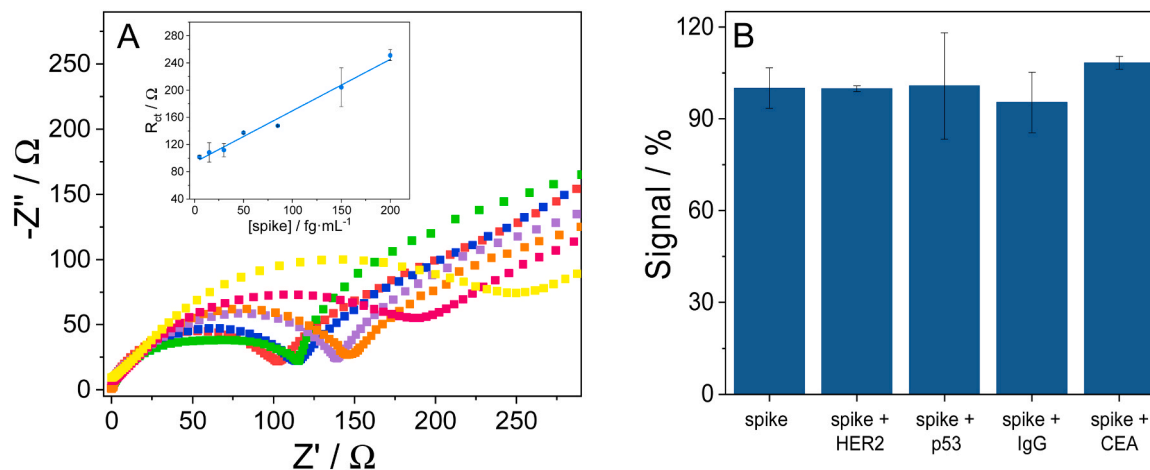


Fig. 5. Nyquist plot and calibration plot (A and inset respectively) of the R<sub>ct</sub> value signal obtained after the incubation with different concentrations (from 5.00 fg/mL to 200 fg/mL) of SARS-CoV-2 S1 protein. Data are presented as mean ± RSD (n = 3). Bar diagram (B) of the percentage variation of the R<sub>ct</sub> value signal obtained for 100 fg/mL of SARS-CoV-2 protein in presence of other interfering proteins such as HER2, p53, IgG, and CEA, at the same concentration.

of 2.10 fg/mL of SARS-CoV-2 S1 protein (minimum concentration detectable by the aptasensor obtained by electrografting of the f-MoS<sub>2</sub> platform), the signal cannot be distinguished from the signal of the control, so the detection of the SARS-CoV-2 S1 protein cannot be assured at this concentration (see **Figure 3SIB**). These results confirm the advantage in sensitivity of using f-MoS<sub>2</sub> electrografted on the GPH SPE surface instead of the p-MoS<sub>2</sub> ones and the relevance of the covalent bonding in the heterostructure.

### 3.4. SARS-CoV-2 S1 protein determination in spiked human serum samples

SARS-CoV-2 S1 protein was determined in spiked human serum samples to study the matrix effect. Based on the biosensor response for three independent determinations of a spiked human serum sample (final SARS-CoV-2 S1 protein concentration of 100 fg/mL), a recovery of 106 % and a RSD of 4 % were obtained. This result demonstrates that the developed aptasensor can be applied for practical applications and has great potential as an alternative to the classical methods of SARS-CoV-2 detection in human samples.

### 3.5. Detection of SARS-CoV-2 S1 protein in nasopharyngeal swab samples

Based on the great interest of having simple methodologies for rapid SARS-CoV-2 S1 protein detection and considering the good results obtained with the developed biosensor in spiked human serum samples, we take a step forward and applied our methodology to detect SARS-CoV-2 S1 protein in spiked nasopharyngeal swab samples as described in detail in experimental section. Differences in the  $R_{ct}$  value of the GPH SPE/f-MoS<sub>2</sub>/apt-SH/BSA platform and the GPH SPE/f-MoS<sub>2</sub>/apt-SH/BSA/PBS + non-doped nasopharyngeal sample were observed due to the matrix effect. Considering these differences ( $\Delta R_{ct} = 33.81 \Omega$ ) we recalculate the  $R_{ct}$  value measured for each doped sample (40.0 and 60.0 fg/mL). From these values and the calibration plot ( $R_{ct} = 0.756 \cdot [S1 \text{ protein}] + 94.0$ ;  $R = 0.987$ ), the concentrations of SARS-CoV-2 S1 protein on each sample was determined to be 47.96 and 59.51 fg/mL. The recovery obtained was 119.90 % and 99.18 %, respectively. Based on the results obtained it is confirmed the ability of the device to detect the virus and quantify the amount of the SARS-CoV-2 S1 protein using spiked nasopharyngeal swab samples.

Finally, to demonstrate, among others, the advantage of the developed aptasensor to detect a small amount of SARS-CoV-2 S1 protein. We have compared the results obtained by our aptasensor with those obtained from a commercial antigen test for the same samples. A negative response was obtained (see **Figure 5SI**).

These results demonstrate once again the high sensitivity and applicability of the developed aptasensor and its potential as an alternative to classical SARS-CoV-2 detection methods.

**Table 2** shows EIS or electrochemical aptasensors and biosensors described in the literature to detect SARS-CoV-2 sequences. As can be observed, the analytical parameters of the developed biosensor compare well with those previously reported in the literature. Moreover, the detection limit is comparable or even better, proving that it can be a simple, easy, and great practical alternative for detecting SARS-CoV-2 at very low concentrations [15,19,31,32].

## 4. Conclusions

A simple, sensible, and selective nanostructured biosensor based on a covalent 2D MoS<sub>2</sub>/graphene heterostructured platform for pathogen detection has been developed. SARS-CoV-2 S1 protein is selected as case of study because the availability of new methodologies to detect this virus is still a great deal of interest. The SARS-CoV-2 S1 protein of the virus is detected by Electrochemical Impedance Spectroscopy (EIS). The developed biosensor is able to detect SARS-CoV-2 with a low

**Table 2**

Comparative with other biosensors for SARS-CoV-2 detection.

Biosensor	Based on	Method	LOD	Reference
EIS aptasensor (spike protein)	GPH SPE/ f-MoS <sub>2</sub>	EIS	2.45 fg/mL	This work
EIS aptasensor (spike protein)	AuNPs/ SPCE	EIS	66 pg/ mL	Abrego-Martínez et al. [31]
Electrochemical aptasensor (spike protein)	SWCNT- SPes	DPV	7 nM	Curti et al. [32]
Photoelectrochemical aptasensor (spike protein)	AuNPs/ Yb-TCPP	PEC	5 pg/ μL	Jiang et al. [19]
Electrochemical DNA biosensor (ORF1ab sequence)	MoS <sub>2</sub> / CSPE	DPV	1.01 pM	Martínez-Periñán et al. [15]

competitive limit of detection of 2.10 fg/mL, and high selectivity against other interfering proteins. A recoveries of 119.90 % and 99.18 % were obtained after evaluating the applicability of the aptasensor to determine the SARS-CoV-2 in spiked nasopharyngeal swab samples, thus confirming its practical application. Covalent modification of the electrodes with the f-MoS<sub>2</sub> by electrografting leads to raise improvements in the developed platform, achieving lower limits of detection and higher stability than those obtained in previous studies using p-MoS<sub>2</sub> flakes as nanomaterial. The heterostructured aptasensor developed can be a simple great potential alternative to the classical methods for SARS-CoV-2 detection.

## CRediT authorship contribution statement

Estefania Enebral Romero has carried out the experiments regarding the aptasensor development. Laura Gutierrez and Rafael del Caño have prepared de MoS<sub>2</sub> functionalized platforms. Tania García-Mendiola, Felix Pariente, and Encarnación Lorenzo have supervised the experimental results regarding the biosensor. Manuel Vazquez and Alicia Naranjo have synthesized the molybdenum disulphide functionalized with a diazonium salt (f-MoS<sub>2</sub>). Manuel Vazquez and I. Jénifer Gómez have characterized the biosensing platform. Emilio Perez has supervised the experimental results related to MoS<sub>2</sub> and has participated in the elaboration of the manuscript. Tania García-Mendiola and Encarnación Lorenzo have coordinated the groups and elaborated the manuscript.

## Declaration of Competing Interest

The authors declare that they have no known competing financial interests or personal relationships that could have appeared to influence the work reported in this paper.

## Data availability

Data will be made available on request.

## Acknowledgements

This work has been financially supported by the Spanish Ministry of Economy and Competitiveness (PID2020-116728RB-I00, PID2020-116661RB-I00, CTQ2015-71955-REDT (ELECTROBIONET)) and Community of Madrid (TRANSNANOAVANSENS, S2018/NMT-4349, and PhotoArt P2018/NMT-4367). E. Enebral thank the financial support of “Nanotecnología para detección del SARS-CoV-2 y sus variantes. NANOCOV” project. IMDEA Nanociencia receives support from the “Severo Ochoa” Programme for Centres of Excellence in R&D (MINECO, Grant CEX2020-001039-S). We also thank the Spanish Ministry of Universities for supporting Laura Gutiérrez-Gálvez with the Formación del Profesorado Universitario (FPU) grant (FPU19/06309).



## Appendix A. Supporting information

Supplementary data associated with this article can be found in the online version at [doi:10.1016/j.snb.2023.134105](https://doi.org/10.1016/j.snb.2023.134105).

## References

- [1] Y. Liu, N.O. Weiss, X. Duan, H.-C. Cheng, Y. Huang, X. Duan, Van der Waals heterostructures and devices, *Nat. Rev. Mater.* 1 (2016) 16042.
- [2] J.A. Robinson, Growing vertical in the flatland, *ACS Nano* 10 (2016) 42–45.
- [3] Z. Cai, B. Liu, X. Zou, H.-M. Cheng, Chemical vapor deposition growth and applications of two-dimensional materials and their heterostructures, *Chem. Rev.* 118 (2018) 6091–6133.
- [4] A.K. Geim, I.V. Grigorieva, Van der Waals heterostructures, *Nature* 499 (2013) 419–425.
- [5] M. Long, E. Liu, P. Wang, A. Gao, H. Xia, W. Luo, B. Wang, J. Zeng, Y. Fu, K. Xu, W. Zhou, Y. Lv, S. Yao, M. Lu, Y. Chen, Z. Ni, Y. You, X. Zhang, S. Qin, Y. Shi, W. Hu, D. Xing, F. Miao, Broadband photovoltaic detectors based on an atomically thin heterostructure, *Nano Lett.* 16 (2016) 2254–2259.
- [6] B. Cho, J. Yoon, S.K. Lim, A.R. Kim, D.-H. Kim, S.-G. Park, J.-D. Kwon, Y.-J. Lee, K.-H. Lee, B.H. Lee, H.C. Ko, M.G. Hahm, Chemical sensing of 2D graphene/MoS<sub>2</sub> heterostructure device, *ACS Appl. Mater. Interfaces* 7 (2015) 16775–16780.
- [7] T. Pham, P. Ramnani, C.C. Villarreal, J. Lopez, P. Das, I. Lee, M.R. Neupane, Y. Rheem, A. Mulchandani, MoS<sub>2</sub>-graphene heterostructures as efficient organic compounds sensing 2D materials, *Carbon* 142 (2019) 504–512.
- [8] M. Vera-Hidalgo, E. Giovannelli, C. Navio, E.M. Pérez, Mild covalent functionalization of transition metal dichalcogenides with maleimides: a “Click” reaction for 2H-MoS<sub>2</sub> and WS<sub>2</sub>, *J. Am. Chem. Soc.* 141 (2019) 3767–3771.
- [9] R. Quirós-Ovies, M. Vázquez Sulleiro, M. Vera-Hidalgo, J. Prieto, I.J. Gómez, V. Sebastián, J. Santamaría, E.M. Pérez, Controlled covalent functionalization of 2H-MoS<sub>2</sub> with molecular or polymeric adlayers, *Chem. – Eur. J.* 26 (2020) 6629–6634.
- [10] M. Vázquez Sulleiro, A. Develioglou, R. Quirós-Ovies, L. Martín-Pérez, N. Martín Sabanés, M.L. Gonzalez-Juarez, I.J. Gómez, M. Vera-Hidalgo, V. Sebastián, J. Santamaría, E. Burzurí, E.M. Pérez, Fabrication of devices featuring covalently linked MoS<sub>2</sub>-graphene heterostructures, *Nat. Chem.* 14 (2022) 695–700.
- [11] S. Gbadamasi, M. Mohiuddin, V. Krishnamurthi, R. Verma, M.W. Khan, S. Pathak, K. Kalantar-Zadeh, N. Mahmood, Interface chemistry of two-dimensional heterostructures – fundamentals to applications, *Chem. Soc. Rev.* 50 (2021) 4684–4729.
- [12] C. Huang, Y. Wang, X. Li, L. Ren, J. Zhao, Y. Hu, L. Zhang, G. Fan, J. Xu, X. Gu, Z. Cheng, T. Yu, J. Xia, Y. Wei, W. Wu, X. Xie, W. Yin, H. Li, M. Liu, Y. Xiao, H. Gao, L. Guo, J. Xie, G. Wang, R. Jiang, Z. Gao, Q. Jin, J. Wang, B. Cao, Clinical features of patients infected with 2019 novel coronavirus in Wuhan, China, *Lancet* 395 (2020) 497–506.
- [13] A.C. Walls, Y.-J. Park, M.A. Tortorici, A. Wall, A.T. McGuire, D. Vesler, Structure, function, and antigenicity of the SARS-CoV-2 spike glycoprotein, *Cell* 181 (2020) 281–292, e6.
- [14] V.M. Corman, O. Landt, M. Kaiser, R. Molenkamp, A. Meijer, D.K. Chu, T. Bleicker, S. Brünink, J. Schneider, M.L. Schmidt, D.G. Mulders, B.L. Haagmans, B. van der Veer, S. van den Brink, L. Wijsman, G. Goderski, J.-L. Romette, J. Ellis, M. Zambon, M. Peiris, H. Goossens, C. Reusken, M.P. Koopmans, C. Drosten, Detection of 2019 novel coronavirus (2019-nCoV) by real-time RT-PCR, *Eurosurveillance*. 25 (2020). <https://www.eurosurveillance.org/content/10.2807/1560-7917.ES.2020.25.3.2000045> (accessed October 27, 2022).
- [15] E. Martínez-Periñán, T. García-Mendiola, E. Enebral-Romero, R. del Caño, M. Vera-Hidalgo, M. Vázquez Sulleiro, C. Navio, F. Pariente, E.M. Pérez, E. Lorenzo, A MoS<sub>2</sub> platform and thionine-carbon nanodots for sensitive and selective detection of pathogens, *Biosens. Bioelectron.* 189 (2021), 113375, <https://doi.org/10.1016/j.bios.2021.113375>.
- [16] C. Pina-Coronado, Á. Martínez-Sobrinho, L. Gutiérrez-Gálvez, R. Del Caño, E. Martínez-Periñán, D. García-Nieto, M. Rodríguez-Peña, M. Luna, P. Milán-Rois, M. Castellanos, M. Abreu, R. Cantón, J.C. Galán, T. Pineda, F. Pariente, Á. Somoza, T. García-Mendiola, R. Miranda, E. Lorenzo, Methylene Blue functionalized carbon nanodots combined with different shape gold nanostructures for sensitive and selective SARS-CoV-2 sensing, *Sens. Actuators B Chem.* 369 (2022), 132217, <https://doi.org/10.1016/j.snb.2022.132217>.
- [17] R. del Caño, T. García-Mendiola, D. García-Nieto, R. Álvaro, M. Luna, H.A. Iniesta, R. Coloma, C.R. Díaz, P. Milán-Rois, M. Castellanos, M. Abreu, R. Cantón, J. C. Galán, T. Pineda, F. Pariente, R. Miranda, Á. Somoza, E. Lorenzo, Amplification-free detection of SARS-CoV-2 using gold nanotriangles functionalized with oligonucleotides, *Microchim. Acta* 189 (2022) 171, <https://doi.org/10.1007/s00604-022-05272-y>.
- [18] L. Gutiérrez-Gálvez, R. del Caño, I. Menéndez-Luque, D. García-Nieto, M. Rodríguez-Peña, M. Luna, T. Pineda, F. Pariente, T. García-Mendiola, E. Lorenzo, Electrochemiluminescent nanostructured DNA biosensor for SARS-CoV-2 detection, *Talanta* 240 (2022), 123203, <https://doi.org/10.1016/j.talanta.2021.123203>.
- [19] Z.W. Jiang, T.T. Zhao, C.M. Li, Y.F. Li, C.Z. Huang, 2D MOF-based photoelectrochemical aptasensor for SARS-CoV-2 spike glycoprotein detection, *ACS Appl. Mater. Interfaces* 13 (2021) 49754–49761, <https://doi.org/10.1021/acsami.1c17574>.
- [20] H.S. Magar, R.Y.A. Hassan, A. Mulchandani, Electrochemical impedance spectroscopy (EIS): principles, construction, and biosensing applications, *Sensors* 21 (2021) 6578, <https://doi.org/10.3390/s21196578>.
- [21] D. Bélanger, J. Pinson, Electrografting: a powerful method for surface modification, *Chem. Soc. Rev.* 40 (2011) 3995, <https://doi.org/10.1039/c0cs00149j>.
- [22] D. Nečas, P. Klapetek, Gwyddion: an open-source software for SPM data analysis, *Open Phys.* 10 (2012). <https://www.degruyter.com/document/doi/10.2478/s11534-011-0096-2/html> (accessed October 27, 2022).
- [23] M.A. Ehsan, S.A. Khan, A. Rehman, Screen-printed graphene/carbon electrodes on paper substrates as impedance sensors for detection of coronavirus in nasopharyngeal fluid samples, *Diagnostics* 11 (2021) 1030, <https://doi.org/10.3390/diagnostics11061030>.
- [24] E.P. Randviir, D.A.C. Brownson, J.P. Metters, R.O. Kadara, C.E. Banks, The fabrication, characterisation and electrochemical investigation of screen-printed graphene electrodes, *Phys. Chem. Chem. Phys.* 16 (2014) 4598, <https://doi.org/10.1039/c3cp55435j>.
- [25] J. Pinson, F. Podvorica, Attachment of organic layers to conductive or semiconductive surfaces by reduction of diazonium salts, *Chem. Soc. Rev.* 34 (2005) 429, <https://doi.org/10.1039/b406228k>.
- [26] X. Chen, C. McGlynn, A.R. McDonald, Two-dimensional MoS<sub>2</sub> catalyzed oxidation of organic thiols, *Chem. Mater.* 30 (2018) 6978–6982, <https://doi.org/10.1021/acs.chemmater.8b01454>.
- [27] K.-C. Lin, B. Jagannath, S. Muthukumar, S. Prasad, Sub-picomolar label-free detection of thrombin using electrochemical impedance spectroscopy of aptamer-functionalized MoS<sub>2</sub>, *Analyst* 142 (2017) 2770–2780, <https://doi.org/10.1039/C7AN00548B>.
- [28] Y.-M. Liu, G.-F. Shi, J.-J. Zhang, M. Zhou, J.-T. Cao, K.-J. Huang, S.-W. Ren, A novel label-free electrochemiluminescence aptasensor based on layered flowerlike molybdenum sulfide-graphene nanocomposites as matrix, *Colloids Surf. B Biointerfaces* 122 (2014) 287–293, <https://doi.org/10.1016/j.colsurfb.2014.07.011>.
- [29] Z. Rahmati, M. Roushani, H. Hosseini, H. Choobin, Electrochemical immunosensor with Cu<sub>2</sub>O nanocube coating for detection of SARS-CoV-2 spike protein, *Microchim. Acta* 188 (2021) 105, <https://doi.org/10.1007/s00604-021-04762-9>.
- [30] A. Erdem, H. Senturk, E. Yildiz, M. Maral, Impedimetric detection based on label-free immunoassay developed for targeting spike S1 protein of SARS-CoV-2, *Diagnostics* 12 (2022) 1992, <https://doi.org/10.3390/diagnostics12081992>.
- [31] J.C. Abrego-Martínez, M. Jafari, S. Chergui, C. Pavel, D. Che, M. Siaz, Aptamer-based electrochemical biosensor for rapid detection of SARS-CoV-2: nanoscale electrode-aptamer-SARS-CoV-2 imaging by photo-induced force microscopy, *Biosens. Bioelectron.* 195 (2022), 113595, <https://doi.org/10.1016/j.bios.2021.113595>.
- [32] F. Curti, S. Fortunati, W. Knoll, M. Giannetto, R. Corradini, A. Bertucci, M. Careri, A folding-based electrochemical aptasensor for the single-step detection of the SARS-CoV-2 spike protein, *ACS Appl. Mater. Interfaces* 14 (2022) 19204–19211, <https://doi.org/10.1021/acsami.2c02405>.

**Estefanía Enebral-Romero** reached the Degree in Chemistry in 2020 from the Universidad Autónoma de Madrid, the Master degree in Clinical Trials Monitoring and Pharmaceutical Development in 2021 from the Universidad Antonio de Nebrija and the Master degree in Industrial Chemistry and Introduction to Chemical Research in 2022 from the Universidad Autónoma de Barcelona. She recently started her PhD in Applied Chemistry at the Universidad Autónoma de Madrid in the research group of Chemical Sensor and Biosensor which PI is Full Professor Encarnación Lorenzo. Her research line is focused on the development of electrochemical (bio)sensors for the detection of different pathogens.

**Laura Gutiérrez Gálvez** obtained the Degree in Chemistry in 2019 from the Universidad Autónoma de Madrid and the Master degree in Applied Chemistry in 2020 from the Universidad Autónoma de Madrid. Since 2020 she is a PhD student at the Applied Chemistry Programme of the Universidad Autónoma de Madrid in the Chemical Sensor and Biosensor group lead by Professor Encarnación Lorenzo. Her current research focuses on the development of electrochemiluminescent (bio)sensors for detection of virus and cancer biomarkers.

**Rafael Del Caño** received his PhD in Chemistry from University of Córdoba in 2019, under the mentorship of Teresa Pineda. Afterwards, he made a postdoctoral stage in Encarnación Lorenzo's group at the Autonomous University of Madrid where he was working on the development of new biosensors. Recently, he has been as postdoctoral researcher at Dr. Joseph Wang's group at the University of California, San Diego, where he has been developing new biosensors related to nutrition and wellness. He is currently affiliated with the University of Córdoba, where his current research direction is the design of new electrochemical biosensors, and the improvement of the analytical and physico-chemical properties of the developed biosensors.

**Manuel Vázquez Sulleiro** obtained in 2013 his degree in Chemistry from the Universidade de Santiago de Compostela. He received his PhD in 2018 under the direction of Prof. Maurizio Prato from the Università degli studi di Trieste. Later, he joined the group of Prof. Emilio M. P é rez at IMDEA Nanociencia. Currently, he is a postdoctoral researcher at CICA from the Universidade da Coruña in the group of Prof. Elena Pazos. His research has been focused on the production and functionalization of 2D and carbon-based materials and their applications in electronics, sensing, and biomedicine.

**Alicia Naranjo Chacón** obtained in 2018 her degree in Chemistry from the Universidad de Castilla-La Mancha. She obtained a Master's degree in Molecular Nanoscience and Nanotechnology in the same university in 2019 under the direction of Dra. Ester Vázquez Fernández-Pacheco and Dra. María Antonia Herrero Chamorro in the study of different hydrogels and carbon-based nanomaterials. Currently, she is a PhD student in the group headed by Prof. Emilio M. Pérez at IMDEA Nanoscience, which research is been focused on the study of microemulsions as a new method of patterning different 2D carbon-based materials, as well as, the interaction between this materials with several polymers and their applications.

**I. Jéniffer Gómez** is currently a Postdoctoral Research Fellow at Centro Interdisciplinar de Química e Bioloxía (CICA) at Universidade da Coruña. She obtained her bachelor's and master's degrees in Chemistry from the Universidade de Santiago de Compostela in 2013–2014. In 2018, she obtained her Ph.D. from the Università degli Studi di Trieste. Afterward, she completed a postdoctoral stage at the Central European Institute of Technology (CEITEC-Masaryk University) and the Department of Condensed Matter Physics from the same university. Her research interests are focused on tailoring low-dimensional materials and their possible use as photocatalysts and biological carriers.

**Félix Pariente Alonso** is Full Professor of Analytical Chemistry at the Universidad Autónoma de Madrid (UAM). He was born in Madrid in 1954. He received his B.S. and Ph. D. degrees in Chemistry in 1976 and 1988, respectively. Between 1992 and 1996 he spent several periods as visiting scientist at the University of Cornell in USA. In 1998 he obtains the degree of permanent assistant professor in the UAM. His research interest includes the design and development of enzyme biosensors and genosensors as well as processes involving electrocatalysis with application to the design of fuel cells and new analytical methods.

**Emilio M. Pérez** is Senior Research Professor and Executive Director for Scientific Outreach at IMDEA Nanociencia. His research interests are focused in three areas: 1)

development of new methods for chemical modification of carbon nanotubes; 2) covalent and noncovalent chemistry of 2D materials; and 3) supramolecular chemistry at the single-molecule level. He is alumnus of the Young Academy of Europe, Member of the Editorial Advisory Board of Fullerenes, Nanotubes and Carbon Nanostructures, (Taylor & Francis), and Associate Editor at Chemistry Squared. He has received several distinctions, including the IUPAC Prize for Young Chemists (2006), the Miguel Catalán Award (2014) and the Universidad Complutense de Madrid Foundation Prize for Science and Technology (2010).

**Tania García-Mendiola** received her bachelor's degree in Chemistry and her PhD degree from Universidad Autónoma de Madrid in 2003 and 2009, respectively. At present, she is associate professor in the Department of Analytical Chemistry and Instrumental Analysis at the UAM. Her research interests include the design of new electrochemical sensors and DNA biosensors and the use of nanomaterials to improve the analytical properties of the developed devices. She is the author/coauthor of more than 41 original research publications.

**María Encarnación Lorenzo** is currently Full Professor in the Department of Analytical Chemistry and Instrumental Analysis at the Universidad Autónoma de Madrid. She received her degree in Chemistry in 1978 and her PhD degree in 1985 from the Universidad Autónoma de Madrid. Afterwards, she made a post-doctoral stage at the Department of Chemistry at Dublin City University. In 1990 she was visiting scientist (NATO Program) to the Department of Chemistry in Cornell University. In 1998 the members of the faculty of Tokio University of Agriculture and Technology invited her as visiting professor to the Department of Applied Chemistry. Actually, she is member of management committee of the Spanish Analytical Chemistry Society. Her research interest is the development of sensors and biosensors for the detection of analytes of environmental, clinical and food interest. She is the author/coauthor of more than 100 original research publications and several book chapters in the area of analytical chemistry.